Proceedings of the ASME 2010 3rd Joint US-European Fluids Engineering Summer Meeting and 8th International Conference on Nanochannels, Microchannels, and Minichannels
FEDSM-ICNMM2010
August 1-5, 2010, Montreal, Canada

FEDSM-ICNMM2010-31106

EFFECTS OF INCREASING INLET VELOCITIES AND SIDE PORT AIR INJECTION ON A BIOMASS FLUIDIZING BED

Mirka Deza and Francine Battaglia*
Department of Mechanical Engineering
Virginia Polytechnic Institute and State University
Blacksburg, Virginia 24061
*fbattaglia@vt.edu

ABSTRACT

Fluidized beds are being used in practice to gasify biomass to create producer gas, a flammable gas that can be used for process heating. However, recent literature has identified the need to better understand and characterize biomass fluidization hydrodynamics, and computational fluid dynamics (CFD) is one approach in this effort. Previous work by the authors considered the validity of using two-dimensional versus three-dimensional simulations to model a cold-flow fluidizing biomass bed configured with a single side port air injection. The side port is introduced to inject air and promote mixing within the bed. Comparisons with experiments indicated that three-dimensional simulations were necessary to capture the fluidization behavior for the more complex geometry. This paper considers the effects of increasing fluidization air flow and side port air flow on the homogeneity of the bed material in a 10.2 cm diameter fluidized bed. Two air injection ports diametrically opposed to each other are also considered to determine their effects on fluidization hydrodynamics. Whenever possible, the simulations are compared to experimental data of time-averaged local gas holdup obtained using X-ray computed tomography. This study will show that increasing the fluidization and side port air flows contribute to a more homogeneous bed. Furthermore, the introduction of two side ports results in a more symmetric gas-solid distribution.

Keywords: Biomass, Computational fluid dynamics, Fluidized bed, Hydrodynamics, Injection port

INTRODUCTION

Fluidized bed gasifiers are found in many industrial processes to convert feedstocks with low-carbon content into valuable products such as fuels, basic chemicals, and hydrogen. Some advantages of fluidized bed operation include nearly isothermal conditions due to rapid mixing of particles, high heat and mass transfer rates and the ability to work with particles of various sizes [1, 2]. The use of biomass in fluidized beds is of current interest because biomass is considered as a renewable alternative energy resource that can potentially provide low cost power production or process heating needs. Effectively fluidizing biomass is extremely important to industries that are using biomass material in gasification processes to yield high quality producer gas. Although biomass gasifiers are being built and used in biorefineries, there are problems with fluidizing the media. Biomass particles are typically difficult to fluidize due to their peculiar shape and a second inert material, such as sand, alumina, or calcite, is typically added to the bed. The large differences in size and density between the biomass and inert particles lead to nonuniform distribution of the biomass within the fluidized bed, and particle interactions and mixing become major issues. Therefore, the fluidization characteristics of biomass particles are of critical importance because of known problems such as particle agglomeration, defluidization, elutriation, and segregation [3–8].

One method to enhance and promote mixing in a fluidized bed is with the inclusion of a side port injection, where either additional gas, biomass or some combination is fed into the re-

actor bed. There have been studies on the effects of injecting gas through a side prot and the influence on fluidization and gasification. Experimental studies of Rajan et al. [9] found that side air injection influenced the circulation pattern of the fluidized bed. Low jet flow promoted mixing and enhanced solid circulation, while high flowrates showed a tendency to increase elutriation, and in small diameter beds, caused slugging. Chyang et al. [10] experimentally studied the modes of gas discharge from a single jet in a two-dimensional (2D) fluidized bed. They identified three regimes for either a bubbling, transition or jetting flow by comparing a modified Froude number and the ratio of nozzle to particle diameter. The bubbling regime was characterized by low Froude number and the jetting regime occurred at high Froude number. Chen and Weinstein [11] numerically and experimentally investigated a 2D fluidized bed with horizontal jet injection. They compared solids void fraction in the jet–influenced area and found three different regions: coherent voids, bubble trains and a zone of surrounding compaction. Another important contribution was made by Xuereb et al. [12] who experimentally determined the penetration length and expansion angle as well as the effects of inlet and jet velocity and particle diameter. They confirmed that close to the injection point, there is a dragging zone of particles from the dense phase into the jet.

Earlier work on horizontal injection mainly focused on finding empirical correlations to measure the jet penetration length [13–15]. Geometric parameters that characterize the injection port, including shape, diameter, and location, and flow conditions such as fluidizing gas velocity and side air injection velocity, have been considered to determine their effects on jet penetration. Hong et al. [16] proposed a correlation for inclined jets, based on Merry's correlation [15] for horizontal jets and validated it with experimental data and numerical simulations using a two-fluid model for fluidization. The influences of gas velocity of the jet, nozzle diameter, inclination, and location were studied in detail. The correlation can be simplified for horizontal jet injection at small angles of inclination. Numerical simulations conducted by Tyler and Mees [17] compared three discretization schemes (Hybrid, Minmod, and Superbee), and found that simulating the bed with the Superbee scheme resulted in bubble and jet behavior, shape, and formation consistent with what was observed in experiments. From their preliminary study with qualitative comparisons, they concluded that three-dimensional (3D) simulations were in best agreement with experiments. More numerical simulations have been done by Li et al. [18] by proposing a scaled Gilbaro drag model in a 3D cylindrical reactor to avoid overprediction of bed expansion and agglomeration of particles in the bed. The results of the simulations were tested quantitatively by comparing the jet penetration length and angle with experiments and three empirical correlations. Li et al [19] also investigated the effects of single and multiple jets in the hydrodynamics of a rectangular fluidized bed. They concluded that multiple jets do not influence each other significantly until they start to overlap. Another conclusion was that gas injection strongly affects the fluid behavior of the bed that is above the injection port when the injection flowrate is relatively high, and side effects are negligible in the part below the injection port. It was also concluded that deep penetration of jet enhanced solid circulation in the core; however deeper penetration could lead to a slugging bed flow.

Two- and three-dimensional simulations of a fluidized bed with side air injection were performed by Deza et al. [20, 21] to determine when two-dimensional simulations are adequate to capture the bed hydrodynamics. From a computational resource point of view, two-dimensional simulations are easier to perform than three-dimensional simulations, but they may not capture the proper physics. Previous work of Xie et al. [22] and Deza et al. [23,24] have shown very good agreement using a 2D approach for a cylinder reactor with no side air injection when the flow is limited to the bubbling regime for Geldart B particles. To examine the influence of side port air injection, glass beads were used for the bed material in the preliminary study [20] because the properties of glass are well-characterized. The simulations for both 2D and 3D representations of the reactor compared well with the experiments. However, when biomass was used as the bed medium [21], in this case ground walnut shell because it is a Geldart B particle, the findings showed that 2D simulations were reasonable for low inlet gas velocities but that nonuniform fluidization resulting from higher inlet gas velocities did not accurately predict the experiments. Thus, it was concluded that in order to best model a biomass reactor with a side port, three-dimensional simulations are necessary. This paper considers the effects of increasing fluidization air flow and side port air flow on the homogeneity of the bed material in a 10.2 cm diameter fluidized bed. Two air injection ports diametrically opposed to each other are also considered to determine their effects on fluidization hydrodynamics. Simulations will be performed for a biomass (walnut) fluidized bed using three-dimensional modeling of the reactor and side port. Whenever possible, the simulations are compared to experimental data of time-averaged local gas holdup obtained using X-ray computed tomography.

NUMERICAL MODEL

A multifluid Eulerian-Eulerian model is employed in Multiphase Flow with Interphase eXchanges (MFIX) [25] and assumes that each phase behaves as interpenetrating continua with its own physical properties. The instantaneous variables are averaged over a region that is larger than the particle spacing but smaller than the flow domain. Volume fractions are introduced to track the fraction each phase occupies in the averaging volume, where ϵ_g is the gas phase volume fraction (also referred to as the void fraction) and ϵ_s is the solid phase volume fraction. Assuming a single gas phase and solid phase, the volume fractions must satisfy the relation that $\epsilon_g + \epsilon_s = 1$. The solid phase is described with an effective particle diameter d_p and characteristic material properties, and solved using a conservation equation

for the solid phase.

The continuity equations for the gas phase and the solid phase, respectively, are:

$$\frac{\partial}{\partial t}(\epsilon_g \rho_g) + \nabla \cdot (\epsilon_g \rho_g \mathbf{u}_g) = 0 \quad (1)$$

$$\frac{\partial}{\partial t}(\epsilon_s \rho_s) + \nabla \cdot (\epsilon_s \rho_s \mathbf{u}_s) = 0 \quad (2)$$

where (ρ) is the density and (**u**) the velocity vector.

The momentum equations for the gas and solid phases have the form:

$$\frac{\partial}{\partial t}(\epsilon_g \rho_g \mathbf{u}_g) + \nabla \cdot (\epsilon_g \rho_g \mathbf{u}_g \mathbf{u}_g) = -\epsilon_g \nabla P_g + \nabla \cdot \bar{\bar{\sigma}}_g + \mathbf{I}_g + \epsilon_g \rho_g \mathbf{g} \quad (3)$$

$$\frac{\partial}{\partial t}(\epsilon_s \rho_s \mathbf{u}_s) + \nabla \cdot (\epsilon_s \rho_s \mathbf{u}_s \mathbf{u}_s) = -\epsilon_s \nabla P_g + \nabla \cdot \bar{\bar{\sigma}}_s - \mathbf{I}_g + \epsilon_s \rho_s \mathbf{g} \quad (4)$$

The expressions on the left side are the net rate of momentum increase and the net rate of momentum transfer by convection. The right side includes contributions for buoyancy caused by the fluid pressure gradient, the stress tensors ($\bar{\bar{\sigma}}$), gravity (**g**), and the interaction forces (**I**) accounting for the momentum transfer between the gas and solid phases; this will be discussed in detail later in this section. The constitutive equations for the gas phase tensor can be found in [25].

The granular temperature θ for the solid phase can be related to the granular energy, defined as the specific kinetic energy of the random fluctuating component of the particle velocity. The resulting transport equation for the granular temperature [26] is:

$$\frac{3}{2}\left[\frac{\partial}{\partial t}(\epsilon_s \rho_s \theta) + \nabla \cdot (\epsilon_s \rho_s \theta)\mathbf{u}_s\right] = \bar{\bar{\sigma}}_s : \nabla \mathbf{u}_s - \nabla \cdot \mathbf{q}_\theta + \gamma_{slip} - \gamma_\theta + \phi_g \quad (5)$$

where $\mathbf{q}_\theta$ is the diffusive flux of granular energy, γ_{slip} is the production of translational fluctuation kinetic energy due to gas-solid slip, γ_θ is the rate of granular energy dissipation due to inelastic collisions [27], and ϕ_g is the transfer of granular energy between the gas phase and solid phase. Since the numerical simulations will model a cold-flow fluidized bed, the energy equation will not be employed in MFIX and therefore is not presented here. For cases where the particle diameter is not perfectly spherical, the particle diameter used in the correlations is modified. The sphericity ψ is the particle property that indicates how spherical a particle is, where $\psi = 1$ is a perfect sphere. Therefore, the modified particle diameter is $d_p = \psi \bar{d}_p$, where $\bar{d}_p$ is the mean diameter and ψ is the estimated sphericity of the actual particles.

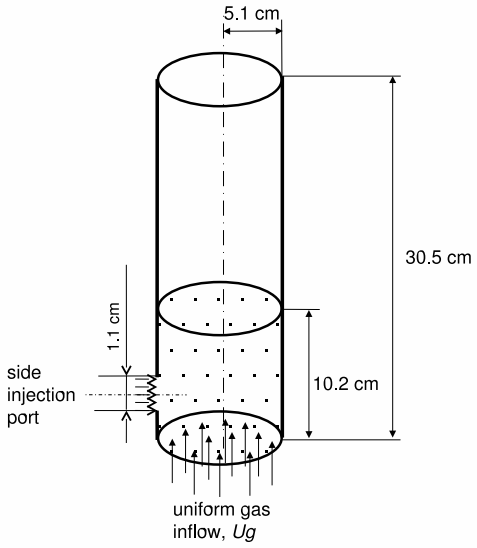

Figure 1: Schematic of the bed chamber and freeboard in a cylindrical reactor, including the side port injector.

Kinetic theory for granular flow is used to calculate the solid stress tensor and solid-solid interaction force in the rapid granular flow regime [25]. There are two distinct flow regimes in granular flow: a viscous or rapidly shearing regime in which stresses arise due to collisional or translational momentum transfer, and a plastic or slowly shearing regime in which stresses arise due to Coulomb friction between solids in close contact. A blending function to provide a smooth transition between each regime is employed [22]. Further details related to the constitutive relations in Eqns. (3-5) can be found in the MFIX theory guide [25].

The interaction force ($\mathbf{I}_g$) in the momentum Eqns. (3) and (4) accounts for the gas-solid momentum transfer, which is expressed as the product of the coefficient for the interphase force between the gas and solid phases and the slip velocity between the two phases. The coefficient for the interphase force is different for each drag model. The Gidaspow model [28] calculates the interphase drag force coefficient using two correlations depending on the local void fraction value and a blending function. For void fractions less than 0.8 the Ergun equation is used to calculate the interphase force coefficient and for void fractions greater than or equal to 0.8 the Wen-Yu equation is used. To avoid a discontinuity between the models, the blending function is introduced. The work herein has employed the Gidaspow model and previous studies by the authors have shown the validity of using the model for glass beads and ground walnut shell [29].

Solution Methodology

To discretize the governing equations in MFIX, a finite volume approach for a staggered grid is used to reduce numerical instabilities [30]. Velocities are stored at the cell surfaces, and scalars, such as void fraction and pressure, are stored at the center

Table 1: Properties and flow characteristics for walnut shell

particle diameter, $\bar{d}_p$ (cm)	0.055
particle density, ρ_p (g/cm^3)	1.3
bulk density, ρ_b (g/cm^3)	0.579
sphericity, ψ (–)	0.6
coefficient of restitution, e (–)	0.85
initial void fraction, ϵ_g^* (–)	0.555
minimum fluidization velocity, U_{mf} (cm/s)	18.4

Table 2: Inlet velocities and side injection flowrates

U_g (cm/s)	Q_{side} (cm^3/s)
$1.5U_{mf}$	0
$3.0U_{mf}$	0
$5.0U_{mf}$	0
$3.0U_{mf}$	$5\%Q_{mf}$
$3.0U_{mf}$	$10\%Q_{mf}$
$3.0U_{mf}$	$20\%Q_{mf}$
$3.0U_{mf}$	2 ports; $5\%Q_{mf}$ each port

of the cell. Discretization of time derivatives are first-order and discretization of spatial derivatives are second-order. An important feature is the use of a second-order discretization scheme for the convective terms, known as the Superbee method [31], which improves convergence and accuracy of the solution. A modification of the SIMPLE algorithm is used to solve the governing equations [30]. The first modification uses an equation for the solid volumes fraction that includes the effect of the solids pressure to help facilitate convergence for a both loosely and densely packed regions. The second modification uses a variable time-stepping scheme to improve convergence and execution speeds.

Problem Description

The fluidized bed reactor used in the experiments consisted of a 10.2 cm diameter, 30.5 cm tall bed chamber with a 61 cm tall chamber above to prevent particle elutriation. Air flows from the plenum through a distributor plate drilled with 62, 0.1 cm diameter holes, where each hole was spaced 1.27 cm apart on a circular grid. The reactor was fashioned with a 1.1 cm diameter side port for air injection (see Fig. 1). X-ray computer tomography (CT) imaging was used to provide time-averaged local and global gas holdup. Complete details of the experimental methods are described by Franka and Heindel [32]. The experiments will be used to help validate the simulations when possible, although the focus of this paper is a CFD investigation. It should be noted that the work herein also explores the use of two side ports, therefore, no experimental data are available. Results will be shown for the lower region within the reactor (up to a height of 30 cm).

For all simulations, air is uniformly provided at the bottom of the domain (see Fig. 1) equal to the superficial gas velocity as a simplification of the flow across the distributor plate in the experiments. The side port injection is also modeled with uniform air velocity at the inlet. The no-slip condition is used to model the gas-wall interactions and a partial-slip condition is used for the particle-wall interactions [33]. Table 1 summarizes the ground walnut shell particle properties and flow conditions. The sphericity and coefficient of restitution were numerically estimated based on previous work by Deza et al. [29], whereas the other properties were provided from the experiments. Three inlet gas velocities are examined; the lowest velocity of $U_g = 1.5U_{mf}$ represents a mild bubbling bed and the higher velocities of $U_g = 3.0$ and $5.0U_{mf}$ represent an industrial reactor flowrate [34]. A base case with no side port air injection ($Q_{side} = 0$) and two additional cases of $Q_{side} = 5\%$ and $10\%Q_{mf}$ are studied, where Q_{mf} is the minimum fluidization volumetric flowrate based on the bed inlet. Finally a comparison using two ports diametrically opposed with $5\%Q_{mf}$ air is studied and a summary of each case is shown in Table 2.

Table 3: Central processing unit information

	2D	3D
CPU (s)	155,200	4,155,000
# time-steps	144,860	272,100
average Δt (s)	0.00044	0.00024
# cells	2400	19,200
μs/time-step/cell	446	795

The grid resolution study by Deza et al. [29] identified a sufficient number of cells that would produce an estimated numerical error less than 1%. The study was for a two-dimensional domain, where a total of 2400 grid cells provided adequate resolution of the domain. The work herein uses a resolution for the 3D domain with 40×60 cells in the radial and axial directions and 16 cells in the azimuthal direction that form parallelepiped cells due to the circular cross-section of the domain. Although the grid resolution may seem coarse, Table 3 compares the computational time required for simulations performed on an AMD Opteron cluster (dual processor, dual core 2.4 GHz AMD 280

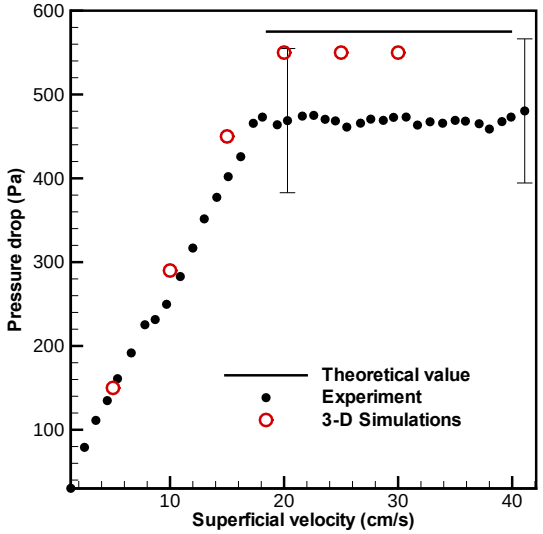

Figure 2: Pressure drop versus superficial gas velocity comparing simulations and experiments for the fluidized bed with no side port (Q_{side} =0).

Opteron). The time-step used by MFIX automatically adjusts to help the simulation converge. The mean time-step for a 3D simulation with $3.0U_{mf}, 10\%Q_{mf}$ was on the order of 0.00024 s. The simulations are time-averaged from 5 to 65 s (which represents the average of 6000 time-steps).

The pressure drop across the ground walnut shell fluidized bed versus the superficial gas inlet velocity when $Q_{side} = 0$ is shown in Fig. 2. The results compare the experimental measurements to that predicted using MFIX. Once the bed is fluidized at $U_{mf} = 18.4$ cm/s, the measured pressure drop is approximately constant at 470 $\pm$ 86 Pa [32] whereas the predicted pressure drop is approximately 560 Pa. It should be noted that the CFD predictions are in very close agreement with the theoretical pressure drop and that the slight discrepancy with experiments is due to error associated with the irregular particle sizes for ground walnut shell. Furthermore, the simulations utilized a single particle diameter of 550 μm, whereas the experiments had a particle diameter range of $500 - 600$ μm.

Inlet Velocity

The effects of increasing inlet velocity on the fluidized bed are compared in Fig. 3, which shows contour plots of the average void fraction for the centerplane of the cylindrical reactor. Three different velocities are presented: $1.5U_{mf}$, $3.0U_{mf}$, and $5.0U_{mf}$ in Fig. 3(a), (b), and (c), respectively. The most obvious trend is that the bed expansion increases with increasing gas velocity at the inlet. Physically, the increasing bed expansion indicates the

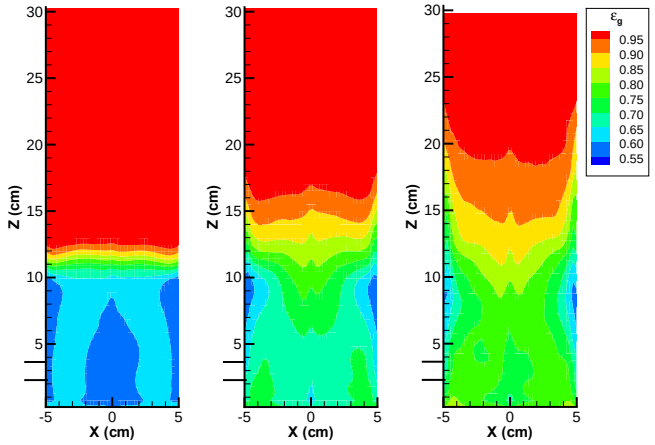

(a) $1.5U_{mf}$ (b) $3.0U_{mf}$ (c) $5.0U_{mf}$

Figure 3: Average void fraction for the fluidized bed with no side port ($Q_{side} = 0$) and (a) $1.5U_{mf}$, (b) $3.0U_{mf}$ and (c) $5.0U_{mf}$.

presence of more gas bubbles (voids) moving through the bed material. It is evident that for inlet velocity of $U_g = 5.0U_{mf}$ the gas–solid distribution is more nonuniform throughout the bed. At low U_g, the solids tend to concentrate along the reactor axis and the walls; this tendency decreases with increasing inlet velocity. With higher inlet velocities, the surface of the bed is less defined and this can be seen in Fig. 3(c), where the void fraction for $5.0U_{mf}$ gradually increases from 0.8 to 1.0 above a height of 11 cm.

Side Injection Flowrate

It has been established that injecting air through a horizontal port promotes mixing in the fluidized bed. The effects of increasing side injection rate at a moderate inlet velocity of $3.0U_{mf}$ will be examined next. Three side injection flowrates of $5\%Q_{mf}$, $10\%Q_{mf}$, and $20\%Q_{mf}$ are presented in Fig. 4 for the void fraction averaged across the reactor cross-sectional area versus axial direction. Results from the experiments are shown as symbols (only for $Q_{side} = 5$ and $10\%Q_{mf}$) and lines are used for the simulation data. In general, the mean void fraction trends are very similar, irrespective of side port air flowrate. With increasing axial position, the mean void fraction is relatively uniform until 10 cm, above which the void fraction gradually increases from 0.7 to 0.9 by 15 cm. Furthermore, the comparisons between the simulations and experiments are in good agreement.

To better understand the mixing trends, the simulations are shown in Figs. 5(a)–(c) as contour plots of the void fraction for the centerplane of the cylindrical reactor through the injection port (upper row) as well as two circular cross-sections located at heights of $z = 3.2$ cm (lower row) and 9.0 cm (middle row).

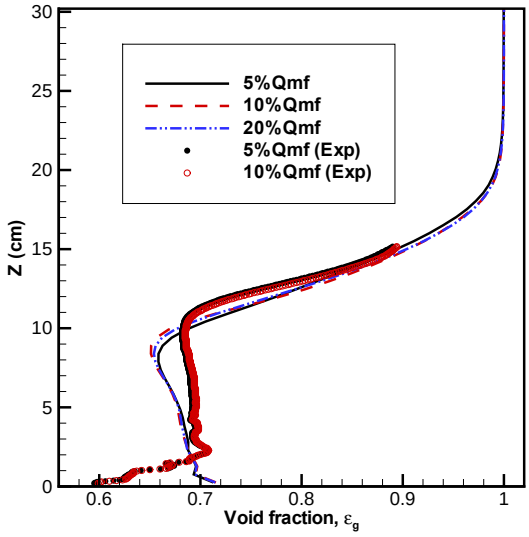

Figure 4: Average void fraction for the $3.0U_{mf}$ fluidized bed and side port injection flowrates of $Q_{side} = 5, 10$ and $20\%Q_{mf}$. Experimental data shown as symbols and simulations are shown as lines.

The gas-solid distribution throughout the centerplane does not vary significantly with increasing side injection, except for the region near the port, where higher void fractions are present for higher side port air injection rates. The circular cross-sections at $z = 3.2$ cm show higher void fractions because additional air injected through the port is present near this height. Annular sections of higher solid volume fraction are observed at $z = 9.0$ cm regions because the solid particles tend to move toward the wall opposite to the port. The void fraction distribution is more uniform with increasing side flowrate.

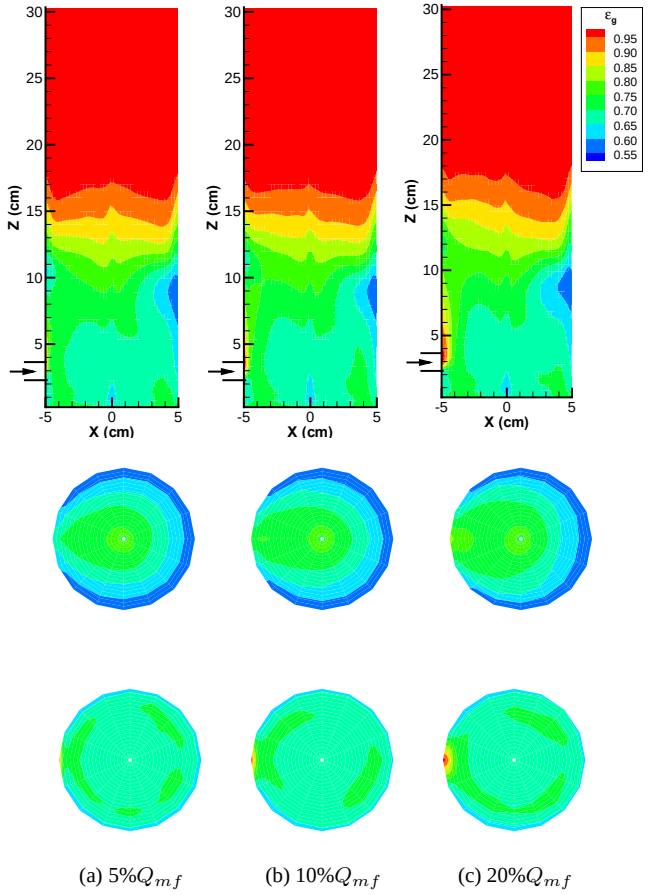

(a) $5\%Q_{mf}$ (b) $10\%Q_{mf}$ (c) $20\%Q_{mf}$

Figure 5: Average void fraction for the $3.0U_{mf}$ fluidized bed using side port injection flowrates of (a) $5\%Q_{mf}$, (b) $10\%Q_{mf}$, and (c) $20\%Q_{mf}$. Upper row are centerplanes through the port, middle row are circular cross-sections at $z = 9.0$ cm and lower row are circular cross-sections at $z = 3.2$ cm.

One versus Two Injection Ports

The medium injection flowrate of $10\%Q_{mf}$ through one port and $5\%Q_{mf}$ through two ports (for a total of $10\%Q_{mf}$) have been further compared in Fig. 6 for the void fraction averaged across the reactor cross-sectional area versus axial direction. As previously mentioned, only one side port was manufactured for the reactor used in the experiments. Results from the experiments are shown as symbols (only for $0\%Q_{mf}$ and $10\%Q_{mf}$ through one side port) and lines are used for the simulation data. As was observed in Fig. 4, the simulations are in good agreement with the experiments and the void fraction is relatively uniform through the bed.

Figure 7(a)–(c) shows contour plots of the void fraction for no side port ($Q_{side} = 0$), one side air injection port with $10\%Q_{mf}$, and two side air injection ports each with $5\%Q_{mf}$, respectively. The upper row is void fraction for the centerplane of the cylindrical reactor containing the injection port and annular sections located at $z = 3.2$ cm (lower row) and 9.0 cm (middle row). The results for no injection port (Figs. 7(a)) shows less homogeneity in the bed above 9 cm. The addition of one side air port increases the fluidization and the particles move toward the opposite wall. However, two side air ports diametrically opposed improve the gas-solid distribution in the bed. It also eliminates the asymmetry of the flow.

In an effort to further quantify and contrast the simulations with the experiments, time-averaged void fraction profiles at two axial locations, $z = 3.2$ and 9 cm, are shown in Fig. 8 for the same cases. The experimental data are shown (symbols) for a slice through the side port. Overall, the 3D predictions for local void fraction profiles compare well with the experiments. There

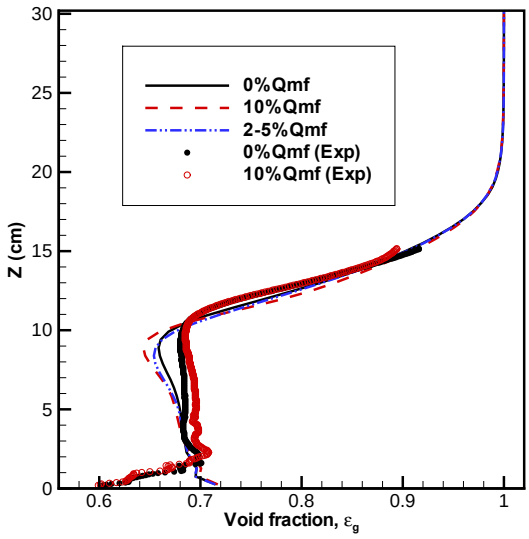

Figure 6: Average void fraction for the $3.0U_{mf}$ fluidized bed with side port injection flowrates of $Q_{side} = 0, 10\ \%Q_{mf}$ and 2 ports with $5\%Q_{mf}$ through each port. Experimental data shown as symbols and simulations are shown as lines.

is a difference for the case with no side air port between the simulations and experiments, and the variations in the experimental data are attributed to the nonuniform inlet conditions that result from the discrete air inlet holes in the distributor plate. Similar discrepancies have been shown by others [35–38]. The void fraction is uniform at lower axial locations (Fig. 8(b)) and with the side ports, the gas-solid distribution is more uniform at higher axial locations (Fig. 8(a)).

Conclusions

The behavior of a biomass fluidizing bed was analyzed using computational fluid dynamics and guidance from published experimental data by Franka and Heindel [32]. Ground walnut shells were used as the biomass medium because it can be characterized as a Geldart B particle. An Eulerian-Eulerian multifluid model was used to simulate and analyze gas-solid hydrodynamic behavior of a fluidized bed. The predictions for pressure drop through the biomass bed were initially validated with the experiments and were found to be in good agreement. The effects of increasing fluidization air flow and side port air flow on the homogeneity of the bed were investigated next. It was found that increasing the inlet velocity at the bottom of the bed positively affected the uniformity of the fluidized bed and increased the overall bed height. Increasing the side port injection flowrate up to $20\%Q_{mf}$ for a single port did not significantly affect the behavior of the bed, and the simulations compared well with the experimental measurements of void fraction. However, the simulations showed that adding a second side port injector on the opposite side of the reactor improved the mixing and overall homogeneity of the fluidized material. It would be of interest to study the effects of adding one additional port, thus having three equally space ports along the circumference of the reactor to further study their effect on the homogeneity of the bed.

Acknowledgments

The authors would like to extend their thanks to Mr. Nathan Franka and Prof. Theodore (Ted) Heindel of Iowa State University for providing the experimental data used in this work.

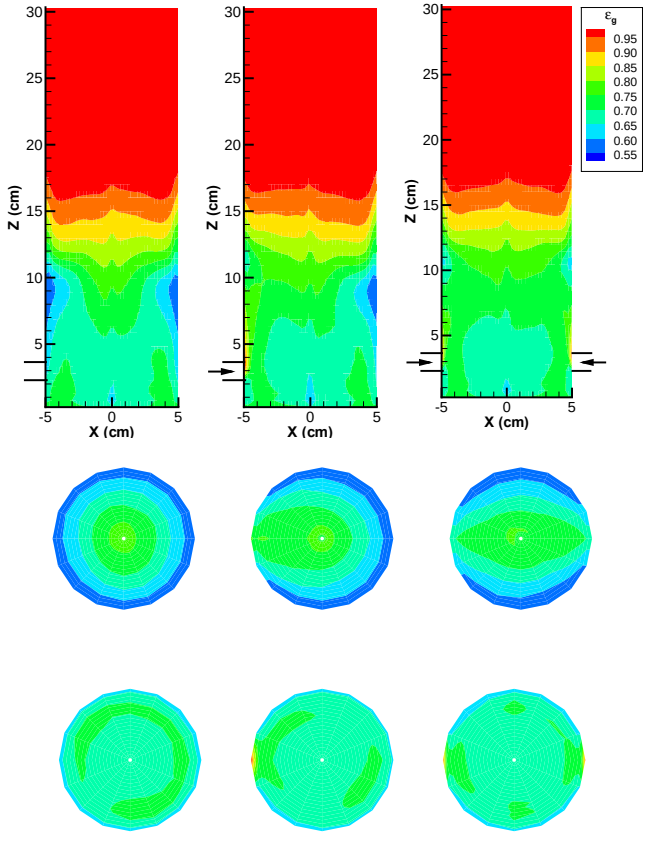

(a) $0\%Q_{mf}$ (b) $10\%Q_{mf}$ (c) 2 ports, $5\%Q_{mf}$

Figure 7: Average void fraction for the $3.0U_{mf}$ fluidized bed using side injection flowrates of (a) $0\%Q_{mf}$, (b) $10\%Q_{mf}$, and (c) 2 ports with $5\%Q_{mf}$, each. Upper row are centerplanes through the port, middle row are circular cross-sections at $z = 9.0$ cm and lower row are circular cross-sections at $z = 3.2$ cm.

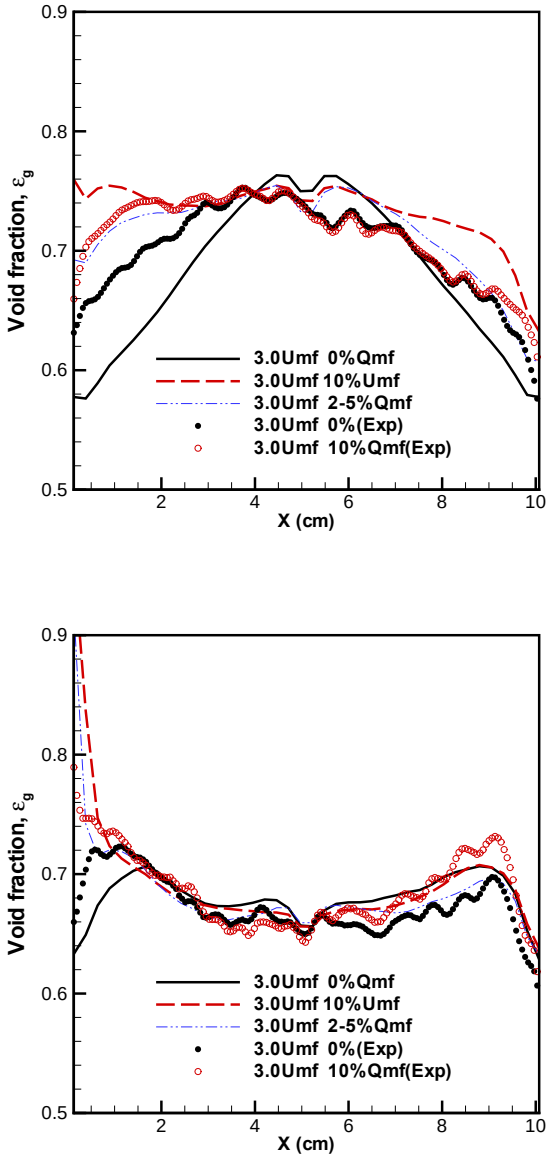

(b) $z = 3.2$ cm

Figure 8: Average void fraction profiles for the $3.0U_{mf}$ fluidized bed with side port injection flowrates of $Q_{side} = 0, 10$ $\%Q_{mf}$ and 2 ports with $5\%Q_{mf}$ through each port at (a) $z = 9.0$ cm and (b) $z = 3.2$ cm. Experimental data shown as symbols and simulations are shown as lines.

REFERENCES

[1] Kunii, D., and Levenspiel, O., 1991. *Fluidization Engineering*. Butterworth-Heinemann, Boston, USA.

[2] Cui, H., and Grace, J. R., 2007. "Fluidization of biomass particles: A review of experimental multiphase flow aspects". *Chemical Engineering Science*, **62**(1–2), pp. 45–55.

[3] Ohman, M., Pommer, L., and Nordin, A., 2005. "Bed agglomeration characteristics and mechanisms during gasification and combustion of biomass fuels". *Energy and Fuels*, **19**(4), pp. 1742–1748.

[4] Scala, F., Chirone, R., and Salatino, P., 2006. "Combustion and attrition of biomass chars in a fluidized bed". *Energy and Fuels*, **20**(1), pp. 91–102.

[5] Chirone, R., Miccio, F., and Scala, F., 2006. "Mechanism and prediction of bed agglomeration during fluidized bed combustion of biomass fuel: Effect of the reactor scale". *Chemical Engineering Journal*, **123**(3), October, pp. 71–80.

[6] Huilin, L., Yunhua, Z., Ding, J., Gidaspow, D., and Wei, L., 2007. "Investigation of mixing/segregation of mixture particles in gas-solid fluidized beds". *Chemical Engineering Science*, **62**(1–2), pp. 301–317.

[7] Nijenhuis, J., Korbee, R., Lensselink, J., Kiel, J. H. A., and van Ommen, J. R., 2007. "A method for agglomeration detection and control in full-scale biomass fired fluidized beds". *Chemical Engineering Science*, **62**(1–2), pp. 644–654.

[8] Bartels, M., Lin, W., Nijenhuis, J., Kapteijn, F., and van Ommen, J. R., 2008. "Agglomeration in fluidized beds at high temperatures: Mechanisms, detection and prevention". *Progress in Energy and Combustion Science*, **34**(5), pp. 633–666.

[9] Rajan, F., and Christoff, J. D., 1992. "Effects of horizontal jet penetration on the combustion of coal in a fluidized bed". *Journal of Energy*, **6**(2), April, pp. 65–70.

[10] Chyand, C. S., Chang, C. H., and Chang, J. H., 1997. "Gas discharge modes at a single horizontal nozzle in a two-dimensional fluidized bed". *Powder Technology*, **90**(1), January, pp. 71–77.

[11] Chen, L., and Weinstein, H., 1993. "Shape and extent of the void formed by a horizontal jet in a fluidized-bed". *AIChE Journal*, **39**(12), pp. 1901–1909.

[12] Xuereb, C., Laguerie, C., and Baron, T., 1991. "Behavior of horizontal or inclined continuous jets gas-injected into a fluidized bed. Part I: Morphology of the jets". *Powder Technology*, **67**(1), pp. 43–56.

[13] Zenz, F. A., 1968. "Bubble formation and grid design". *IChemE Symposium Series*, **30**, pp. 136–139.

[14] Shakhova, N. A., 1968. "Discharge of turbulent jets into a fluidized bed". *Journal of Engineering Physics and Thermophysics*, **14**(1), pp. 32–36.

[15] Merry, J., 1971. "Penetration of a horizontal gas jet into a fluidised bed". *Transactions of the Institution of Chemical Engineers*, **49**(4), pp. 189–195.

[16] Hong, R., Li, H., Li, H., and Wang, Y., 1997. "Studies on the inclined jet penetration length on a gas-solid fluidized bed". *Powder Technology*, **92**(3), pp. 205–212.

[17] Tyler, J., and Mees, P., 1999. "Using CFD to model the interaction of a horizontal feed jet on fluidized bed hydro-

dynamics". In Second International Conference on CFD in the Minerals and Process Industries, CSIRO, Melbourne, pp. 113–117.

[18] Li, T., Pougatch, K., Salcudean, M., and Grecov, D., 2008. "Numerical simulation of horizontal jet penetration in a three-dimensional fluidized bed". *Powder Technology,* **184**, pp. 89–99.

[19] Li, T., Pougatch, K., Salcudean, M., and Grecov, D., 2009. "Numerical simulation of single and multiple gas jets in bubbling fluidized beds". *Chemical Engineering Science,* **64**, pp. 4884–4898.

[20] Deza, M., Battaglia, F., and Heindel, T. J., 2008. "Approximating a three-dimensional fluidized bed with two-dimensional simulations". In Proceedings of the 2008 ASME International Mechanical Engineering Congress and Exposition. Paper IMECE2008-66378.

[21] Deza, M., Heindel, T. J., and Battaglia, F., 2009. "Modeling a biomass fluidizing bed with side port air injection". In Proceedings of the 2009 ASME Fluids Engineering Division Summer Conference. Paper FEDSM2009-78372.

[22] Xie, N., Battaglia, F., and Pannala, S., 2008. "Effects of using two- versus three-dimensional computational modeling of fluidized beds: Part I, hydrodynamics". *Powder Technology,* **182**(1), February, pp. 1–13.

[23] Deza, M., Battaglia, F., and Heindel, T. J., 2007. "Computational modeling of biomass in a fluidized bed gasifier". In Proceedings of the 2007 ASME International Mechanical Engineering Congress and Exposition, IMECE 2007, Vol. **8** PART A, pp. 107–114. Paper IMECE2007-43097.

[24] Deza, M., Battaglia, F., and Heindel, T. J., 2008. "A validation study for the hydrodynamics of biomass in a fluidized bed". In Proceedings of the 2008 ASME Fluids Engineering Division Summer Conference. Paper FEDSM2008-55158.

[25] Syamlal, M., Rogers, W., and O'Brien, T., 1993. MFIX Documentation: Theory Guide. Technical Note DOE/METC-95/1013 and NTIS/DE95000031, National Energy Technology Laboratory, Department of Energy.

[26] Agrawal, K., Loezos, P. N., Syamlal, M., and Sundaresan, S., 2001. "The role of meso-scale structures in rapid gas-solid flows". *Journal of Fluid Mechanics,* **445**, pp. 151–185.

[27] Lun, C. K., Savage, S. B., Jeffrey, D. J., and Chepurniy, N., 1984. "Kinetic theories for granular flow: Inelastic particles in Couette flow and slightly inelastic particles in a general flowfield". *Journal of Fluid Mechanics,* **140**, March, pp. 223–256.

[28] Huilin, L., and Gidaspow, D., 2003. "Hydrodynamics of binary fluidization in a riser: CFD simulation using two granular temperatures". *Chemical Engineering Science,* **58**(16), pp. 3777–3792.

[29] Deza, M., Franka, N. P., Heindel, T. J., and Battaglia, F., 2009. "CFD modeling and X-ray imaging of biomass in a fluidized bed". *Journal of Fluids Engineering,* **131**(11), November, pp. 111303– 1–11.

[30] Syamlal, M., 1998. MFIX Documentation: Numerical Technique. Technical Note DOE/MC31346-5824 and NTIS/DE98002029, National Energy Technology Laboratory, Department of Energy.

[31] Syamlal, M., 1998. High Order Discretization Methods for the Numerical Simulation of Fluidized Beds. Technical Note DOE/FETC/C-98/7305 and CONF-971113, Department of Energy.

[32] Franka, N., and Heindel, T., 2009. "Local time-averaged gas holdup in a fluidized bed with side air injection using X-ray computed tomography". *Powder Technology,* **193**, pp. 69–78.

[33] Johnson, P. C., and Jackson, R., 1987. "Frictional-collision constitutive relations for granular materials with application to plane shearing". *Journal of Fluid Mechanics,* **176**, pp. 67–93.

[34] Reardon, J., 2007. Better biomass gasification for the ethanol industry. Personal Communication: A Presentation by Frontline BioEnergy to T.J. Heindel, October 16.

[35] Taghipour, F., Ellis, N., and Wong, C., 2005. "Experimental and computational study of gas-solid fluidized bed hydrodynamics". *Chemical Engineering Science,* **60**(24), December, pp. 6857–6867.

[36] Du, W., Bao, X., Xu, J., and Wei, W., 2006. "Computational fluid dynamics (CFD) modeling of spouted bed: Assessment of drag coefficient correlations". *Chemical Engineering Science,* **61**(5), March, pp. 1401–1420.

[37] Cao, J., Cheng, Z., Fang, Y., Jing, H., Huang, J., and Wang, Y., 2008. "Simulation and experimental studies on fluidization properties in a pressurized jetting fluidized bed". *Powder Technology,* **183**(1), pp. 127–132.

[38] Ahuja, G. N., and Patwardhan, A. W., 2008. "CFD and experimental studies of solids hold-up distribution and circulation patterns in gas-solid fluidized beds". *Chemical Engineering Journal,* **143**(1–3), pp. 147–160.